

Relaxation of a dewetting contact line

Part 1: A full-scale hydrodynamic calculation

By **JACCO H. SNOEIJER, BRUNO ANDREOTTI,**
GILES DELON AND MARC FERMIGIER

Physique et Mécanique des Milieux Hétérogènes, ESPCI, 10 rue Vauquelin, 75231 Paris Cedex 05, France

(Received 1 February 2008)

The relaxation of a dewetting contact line is investigated theoretically in the so-called "Landau-Levich" geometry in which a vertical solid plate is withdrawn from a bath of partially wetting liquid. The study is performed in the framework of lubrication theory, in which the hydrodynamics is resolved at all length scales (from molecular to macroscopic). We investigate the bifurcation diagram for unperturbed contact lines, which turns out to be more complex than expected from simplified 'quasi-static' theories based upon an apparent contact angle. Linear stability analysis reveals that below the critical capillary number of entrainment, Ca_c , the contact line is linearly stable at all wavenumbers. Away from the critical point the dispersion relation has an asymptotic behaviour $\sigma \propto |q|$ and compares well to a quasi-static approach. Approaching Ca_c , however, a different mechanism takes over and the dispersion evolves from $\sim |q|$ to the more common $\sim q^2$. These findings imply that contact lines can not be treated as universal objects governed by some effective law for the macroscopic contact angle, but viscous effects have to be treated explicitly.

1. Introduction

Wetting and dewetting phenomena are encountered in a variety of environmental and technological contexts, ranging from the treatment of plants to oil-recovery and coating. Yet, their dynamics can not be captured within the framework of classical hydrodynamics – with the usual no-slip boundary condition on the substrate – since the viscous stress diverges at the contact line (Huh & Scriven 1971, Dussan et al. 1974). The description of moving contact lines has remained a great challenge, especially because it involves a wide range of length scales. In between molecular and millimetric scales, the strong viscous stresses are balanced by capillary forces. In this zone, the slope of the free surface varies logarithmically with the distance to the contact line so that the interface is strongly curved, even down to small scales (Voinov 1976, Cox 1986). Ultimately, the intermolecular forces due to the substrate introduce the physical mechanism that cuts off this singular tendency (Voinov 1976, Cox 1986, de Gennes 1986, Blake et al. 1995, Pismen & Pomeau 2000).

A popular theoretical approach has been to assume that all viscous dissipation is localized at the contact line, so that macroscopically the problem reduces to that of a static interface that minimizes the free energy. In such a quasi-static approximation one does not have to deal explicitly with the contact line singularity: the dynamics is entirely governed by an *apparent contact angle* θ_a that serves as a boundary condition for the inter-

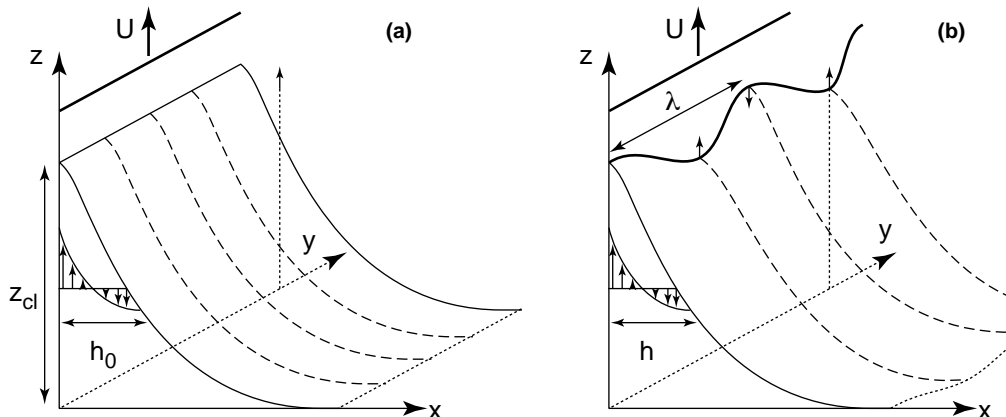


FIGURE 1. (a) A standard geometry to study contact line dynamics is that of a vertical solid plate withdrawn from a bath of liquid with a constant velocity U . The position of the contact line is indicated by z_{cl} . (b) In this paper we study the relaxation of transverse perturbations of contact lines, by computing the evolution of the interface profile $h(z, y, t)$.

face (Voinov 1976, Cox 1986, Joanny & de Gennes 1984, Golestanian & Raphael 2001b, Nikolayev & Beysens 2003). This angle is a function of the capillary number $Ca = \eta U / \gamma$, which compares the contact line velocity U to the capillary velocity γ / η , where γ and η denote surface tension and viscosity. Since the dissipative stresses are assumed to be localized at the contact line, viscous effects will modify the force balance determining the contact angle. This induces a shift with respect to the equilibrium value θ_e . Within this approximation, the difficulty of the contact line problem is hidden in the relation $\theta_a(Ca)$, which depends on the mechanism releasing the singularity. While it is agreed upon that the angle increases with Ca for advancing contact lines and decreases in the receding case, there are many different theories for the explicit form (Voinov 1976, Cox 1986, de Gennes 1986, Blake et al. 1995).

Experimentally, however, it has turned out to be very difficult to discriminate between the various theoretical proposals (Hoffman 1975, Le Grand et al. 2005, Rio et al. 2005). All models predict a nearly linear scaling of the contact angle in a large range of Ca and the prefactor is effectively an adjustable parameter (namely the logarithm of the ratio between a molecular and macroscopic length). Differences become more pronounced close to the so-called forced wetting transition: it is well known that the motion of *receding* contact lines is limited by a maximum speed beyond which liquid deposition occurs (Blake & Ruschak 1979, de Gennes 1986). An example of this effect is provided by drops sliding down a window. At high velocities, these develop singular cusp-like tails that can emit little droplets (Podgorski et al. 2001, Le Grand et al. 2005). Similarly, solid objects can be coated by a non-wetting liquid when withdrawn fast enough from a liquid bath (Blake & Ruschak 1979, Quéré 1991, Sedev & Petrov 1991), see Fig. 1a. Above the transition, a capillary ridge develops (Snoeijer et al. 2006) that eventually leaves a Landau-Levich film of uniform thickness (Landau & Levich 1942).

An important question is to what extent a quasi-static approximation, in which dissipative effects are taken localized at the contact line, are able to describe these phenomena. Only recently, the problem has been addressed by using a fully hydrodynamic model that properly incorporates viscous effects at all length scales (Hocking 2001, Eggers 2004, Eggers 2005). It was found that stationary meniscus solutions cease to exist above a critical value Ca_c , due to a matching problem at both ends of the scale range: the highly

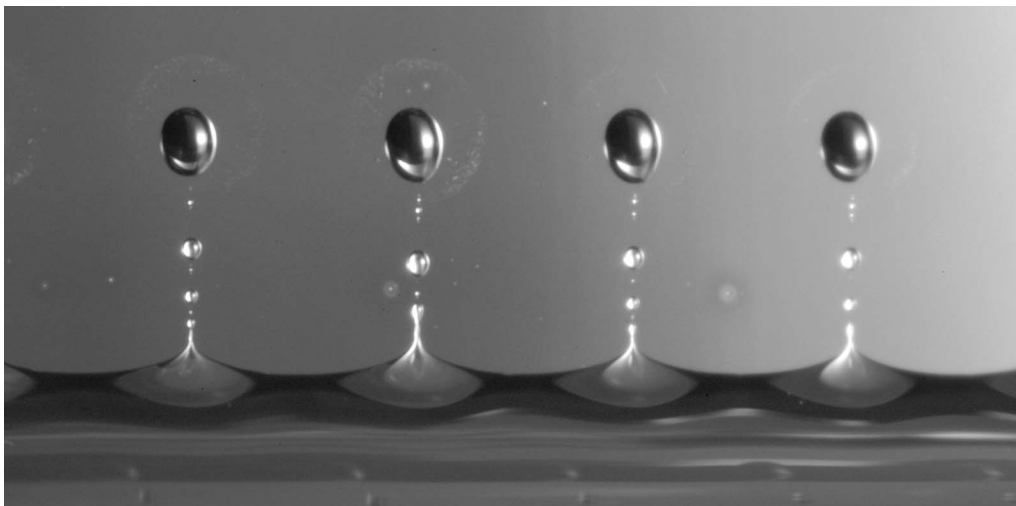


FIGURE 2. Experimental realization of contact line perturbations. The contact line is deformed by "wetting defects" on the partially wetting plate. The narrow connection between the defect and the bath undergoes a Rayleigh-Plateau-like instability, leaving a periodically deformed contact line.

curved contact line zone and the macroscopic flow (Eggers 2004, Eggers 2005). An interesting result of this work is that both the value of Ca_c and the emerging $\theta_a(Ca)$ are not universal: these depend on the inclination at which the plate is withdrawn from the liquid reservoir. Hence, the large scale geometry of the interface *does* play a role and the dynamics of contact lines can not be captured by a single universal law for $\theta_a(Ca)$.

Golestanian and Raphael identified another sensitive test to discriminate contact line models (Golestanian & Raphael 2001a, Golestanian & Raphael 2001b). They considered the relaxation of dewetting contact lines perturbed at a well-defined wave number q , as shown in Fig. 1b. This can be achieved experimentally by introducing wetting defects on the solid plate, separated by a wavelength λ (Ondarçuhu & Veyssié 1991). As can be seen in Fig. 2, these defects create a nonlinear perturbation when passing through the contact line, but eventually the relaxation occurs along the Fourier mode with $q = 2\pi/\lambda$ (Delon et al. 2006). Using a quasi-static theory, Golestanian and Raphael predict that the perturbations decay exponentially $\sim e^{-\sigma t}$ with a relaxation rate

$$\sigma = |q| \frac{\gamma}{\eta} f(Ca) , \quad (1.1)$$

where $f(Ca)$ is very sensitive to the form of $\theta_a(Ca)$. Their theory is built upon the work by Joanny & de Gennes 1984, who already identified the scaling proportional to $|q|$ for static contact lines ($Ca = 0$). Ondarçuhu and Veyssié experimentally confirmed this $|q|$ dependence in the limit of $Ca = 0$ (Ondarçuhu & Veyssié 1991), while more recently, it has been argued that this scaling should saturate to the inverse capillary length $l_\gamma = \sqrt{\gamma/\rho g}$ in the large wavelength limit (Nikolayev & Beysens 2003). However, an intriguing and untested prediction for the *dynamic* problem is that the relaxation times diverge when approaching forced wetting transition at Ca_c . This "critical" behavior should occur at all length scales and is encountered in the prefactor $f(Ca)$, which vanishes as $Ca \rightarrow Ca_c$.

In this paper we perform a fully hydrodynamic analysis of perturbed menisci when a vertical plate is withdrawn from a bath of liquid with a velocity U (Fig. 1). Using the

lubrication approximation it is possible to take into account the viscous dissipation at all length scales, from molecular (i.e. the slip length) to macroscopic. We thus drop the assumptions of quasi-static theories and describe the full hydrodynamics of the problem. The first step is to compute the unperturbed meniscus profiles as a function of the plate velocity. We show that these basic solutions undergo a remarkable series of bifurcations that link the effect that stationary cease to exist beyond Ca_c (Eggers 2004), to the recently observed upward propagating fronts beyond the transition (Snoeijer et al. 2006). Then we study the dispersion of contact line perturbations through a linear stability analysis. Our main findings are: (i) the relaxation time for the mode $q = 0$ scales as $|\text{Ca} - \text{Ca}_c|^{-1/2}$; (ii) finite wavelength perturbations always decay in a finite time even right at the critical point; (iii) the scaling $\sigma \propto |q|$ proposed by Eq. (1.1) breaks down when approaching Ca_c . These results illustrate the limitations of simplified theories based upon an apparent contact angle.

The paper is organized as follows. In Sec. 2 we summarize the results from a quasi-static theory and generalize the work by Golestanian & Raphael. The heart of the paper starts in Sec. 3 where we formulate the hydrodynamic approach and compute the bifurcation diagram of the base solutions. After addressing technical points of the linear stability analysis in Sec. 4, we present our numerical results for the dispersion relation in Sec. 5. The paper closes with a discussion in Sec. 6.

2. Results from quasi-static theory

We briefly revisit the quasi-static approach to contact line perturbations, which will serve as a benchmark for the full hydrodynamic calculation starting in Sec. 3. The results below are based upon the analysis of Golestanian & Raphael, which has been extended to long wavelengths and large contact angles.

2.1. Short wavelengths: $ql_\gamma \gg 1$

At distances well below the capillary length, $l_\gamma = \sqrt{\gamma/\rho g}$, we can treat the unperturbed profiles as a straight wedge of angle θ_a . Perturbations should not affect the total Laplace pressure, and hence not the total curvature of the free interface. The interface will thus be deformed as sketched in Fig. 3a: the advanced part of the contact line has a smaller apparent contact angle than the unperturbed θ_a . According to $\theta_a(\text{Ca})$, such a smaller angle corresponds to a higher velocity with respect to the plate, hence the perturbation will decay. From this argument one readily understands that the rate of relaxation σ , depends on how a variation of θ induces a variation of Ca , and thus involves the derivative $d\text{Ca}/d\theta_a$ (Golestanian & Raphael 2003).

Working out the mathematics, see Appendix B, we find

$$\frac{\eta\sigma}{|q|\gamma} = -\frac{\tan\theta_a}{\cos\theta_a} \left(\frac{d\tan\theta_a}{d\text{Ca}} \right)^{-1}. \quad (2.1)$$

This implies that the timescale for the relaxation is set by the length q^{-1} and the capillary velocity γ/η , where γ represents surface tension and η is the viscosity. We therefore introduce

$$\sigma_\infty(\text{Ca}) = \lim_{ql_\gamma \rightarrow \infty} \frac{\sigma}{ql_\gamma} \frac{\eta l_\gamma}{\gamma}, \quad (2.2)$$

which will be used later on to compare to the hydrodynamic calculation in the limit of large q .

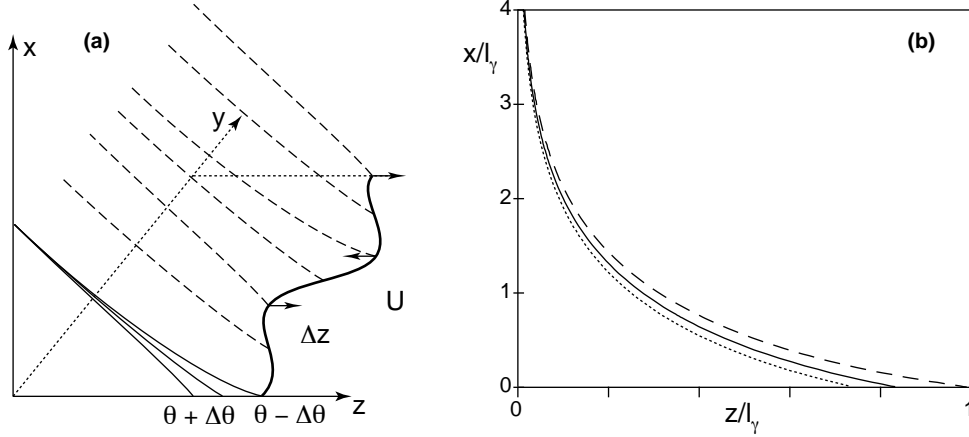


FIGURE 3. (a) Macroscopic representation of the interface shape near a perturbed contact line. The advanced part of the contact line has a smaller apparent contact angle than the unperturbed θ_a , and will thus have a higher speed with respect to the plate. This will decrease the amplitude of the perturbation. (b) Cross-sections of the perturbed interface profile along z . Note that the interface joins the static bath at $z = 0$.

2.2. Large wavelengths: $ql_\gamma \ll 1$

When considering modulations of the contact line with $1/q$ of the order of the capillary length, one can no longer treat the basic profile as a simple wedge. Instead, one has to invoke the full profile $h_0(z)$ and the results for σ are no longer geometry independent (see also Sekimoto et al. 1987). For the geometry of a vertical plate immersed in a bath of liquid, we can characterize the profiles by the "meniscus rise", indicating the position of the contact line z_{cl} above the liquid bath (Fig. 1). This is directly related to the contact angle as (Landau & Lifschitz 1959)

$$z_{cl} = \pm l_\gamma \sqrt{2(1 - \sin \theta_a)}, \quad (2.3)$$

where the sign depends on whether $\theta_a < \pi/2$ (positive), $\theta_a > \pi/2$ (negative). In fact, this relation is often used to experimentally determine $\theta_a(\text{Ca})$, since the meniscus rise $z_{cl}(\text{Ca})$ can be measured more easily than the slope of the interface.

We now consider the relaxation rate σ_0 for perturbations with $q = 0$. Such a perturbation corresponds to a uniform translation of the contact line with Δz . Using the empirical relation $z_{cl}(\text{Ca})$, we can directly write

$$\frac{d\Delta z}{dt} = -\frac{\gamma}{\eta} \Delta \text{Ca} = -\frac{\gamma}{\eta} \left(\frac{dz_{cl}}{d\text{Ca}} \right)^{-1} \Delta z. \quad (2.4)$$

Hence,

$$\frac{\eta l_\gamma \sigma_0}{\gamma} = l_\gamma \left(\frac{dz_{cl}}{d\text{Ca}} \right)^{-1}. \quad (2.5)$$

In terms of the contact angle, using Eq. (2.3), this becomes

$$\frac{\eta l_\gamma \sigma_0}{\gamma} = -\frac{\sqrt{2(1 - \sin \theta_a)}}{|\cos^3 \theta_a|} \left(\frac{d \tan \theta_a}{d\text{Ca}} \right)^{-1}. \quad (2.6)$$

Besides some geometric factors, this result has the same structure as the relaxation for small wavelengths, Eq. (2.1). The crucial difference, however, is that the length scale of the problem is now l_γ instead of q . Comparing the relaxation of finite wavelengths, σ_q ,

with the zero mode relaxation, σ_0 , we thus find

$$\frac{\sigma_q}{\sigma_0} \simeq ql_\gamma g(\theta_a) \quad \text{for } ql_\gamma \gg 1, \quad (2.7)$$

where the prefactor $g(\theta_a)$ reads

$$g(\theta_a) = \frac{|\cos \theta_a| \sin \theta_a}{\sqrt{2(1 - \sin \theta_a)}}. \quad (2.8)$$

Using the definition Eq. (2.2) we thus find the quasi-static prediction

$$\sigma_\infty = \sigma_0 g(\theta_a). \quad (2.9)$$

2.3. Physical implications and predictions

The predictions of the quasi-static approach can be summarized by Eqs. (2.1), (2.5), and (2.9). The relation $\sigma \propto |q|$ was already found by Joanny & de Gennes 1984, who referred to this as the "anomalous elasticity" of contact lines. The linear dependence on q contrasts with the more generic scaling q^2 for diffusive systems, and has been confirmed experimentally by Ondarçuhu & Veyssié 1991 in the static limit, $\text{Ca} = 0$. An interesting consequence is that the Green's function corresponding to this dispersion relation is a Lorentzian $\propto (1 + [y/w(t)]^2)^{-1}$, whose width $w(t)$ grows linearly in time. The prediction is thus that a localized deformation of the contact line, similar to Fig. 2 but now for a single defect, will display a broad power-law decay along y . In the hydrodynamic calculation below we will identify a breakdown of this phenomenology in the vicinity of the critical point.

On the level of the speed-angle law $\theta_a(\text{Ca})$, the wetting transition manifests itself through a maximum possible value of Ca , i.e. $d\theta/d\text{Ca} = \infty$. According to Eqs. (2.1) and (2.6), this suggests a diverging relaxation time σ^{-1} at all length scales. Assume that the scaling close to the maximum is $\theta_a - \theta_c \propto (\text{Ca}_c - \text{Ca})^\beta$, where generically one would expect $\beta = 1/2$. If the critical point occurs at zero contact angle, $\theta_c = 0$, Eq. (2.1) yields a scaling $\sigma_q \propto (\text{Ca}_c - \text{Ca})$ for the case of large q . For $q = 0$ or when $\theta_c \neq 0$, one finds $\sigma_q \propto (\text{Ca}_c - \text{Ca})^{1-\beta}$. Below we show that the mode $q = 0$ indeed displays the latter scaling with $\beta = 1/2$. However, the relaxation times of finite q perturbations always remain finite according to the full hydrodynamic calculation, even at the critical point.

3. Hydrodynamic theory: the basic profile $h_0(z)$

This section describes the hydrodynamic theory that is used to study the relaxation problem. After presenting the governing equations, we reveal the nontrivial bifurcation diagram of the stationary solutions, $h_0(z)$, for different values of the capillary number. This allows an explicit connection between the work on the existence of stationary menisci (Hocking 2001, Eggers 2004, Eggers 2005), and recently observed transient states in the deposition of the Landau-Levich film (Snoeijer et al. 2006). All results presented below have been obtained through numerical resolution of the hydrodynamic equations using a Runge-Kutta integration method.

3.1. The lubrication approximation

We consider the coordinate system (z, y) attached to the solid plate, as indicated in Fig. 1. The position of the liquid/vapor interface is denoted by the distance from the plate $h(z, y, t)$. To really cover the range of length scales from molecular to millimetric, the standard approach is to describe the hydrodynamics using the lubrication approximation

(Oron et al. 1997). This is a long wavelength expansion of the Stokes flow based upon $\text{Ca} \ll 1$, which reduces the free boundary problem to a single partial differential equation for $h(z, y, t)$. Of course, one still has to deal explicitly with the fact that viscous forces tend to diverge as $h \rightarrow 0$. Here we resolve the singularity by introducing a Navier slip boundary condition at the plate,

$$v_z = l_s \frac{\partial v_z}{\partial x} , \quad (3.1)$$

that is characterized by a slip length l_s . Such a slip law has been confirmed experimentally, yielding values for l_s ranging from a single molecular length up to a micron depending on wetting properties of the liquid and roughness of the solid (Barrat & Bocquet 1999, Cottin-Bizonne et al. 2005, Pit et al. 2000, Thompson & Robbins 1989). Different mechanisms releasing the contact line singularity will lead to similar qualitative results, as long as the microscopic and macroscopic lengths remain well separated.

The lubrication equation with slip boundary condition reads (Oron et al. 1997)

$$\partial_t h + \nabla \cdot (h \mathbf{U}) = 0 , \quad (3.2)$$

$$\gamma \nabla \kappa - \rho g \mathbf{e}_z + \frac{3\eta(U \mathbf{e}_z - \mathbf{U})}{h(h + 3l_s)} = \mathbf{0} . \quad (3.3)$$

Here U is the plate velocity, $\mathbf{U}(z, y, t) = U_z \mathbf{e}_z + U_y \mathbf{e}_y$ is the depth-averaged fluid velocity inside the film, while $\nabla = \mathbf{e}_z \partial_z + \mathbf{e}_y \partial_y$. The first equation is mass conservation, while the second represents the force balance between surface tension γ , gravity ρg , and viscosity η , respectively. We maintain the full curvature expression

$$\kappa = \frac{(1 + \partial_y h^2) \partial_{zz} h + (1 + \partial_z h^2) \partial_{yy} h - 2 \partial_y h \partial_z h \partial_{yz} h}{(1 + \partial_z h^2 + \partial_y h^2)^{3/2}} , \quad (3.4)$$

which allows a proper matching to the liquid reservoir away from the contact line.

In the remainder we rescale all lengths by the capillary length $l_\gamma = \sqrt{\gamma/\rho g}$, and all velocities by γ/η , yielding the dimensionless equations

$$\partial_t h + \nabla \cdot (h \mathbf{U}) = 0, \quad (3.5)$$

$$\nabla \kappa - \mathbf{e}_z + \frac{3(\text{Ca} \mathbf{e}_z - \mathbf{U})}{h(h + 3l_s)} = \mathbf{0}. \quad (3.6)$$

The timescale in this equation thus becomes $\eta l_\gamma / \gamma$.

3.2. Boundary conditions

We now have to specify boundary conditions at the liquid reservoir and at the contact line – see Fig. 3. Far away from the plate, $h \rightarrow \infty$, the free surface of the bath is unperturbed by the contact line. Defining the vertical position of the bath at $z = 0$, we can thus impose the asymptotic boundary conditions as $z \rightarrow 0$

$$\begin{aligned} \partial_z h &= -\infty, \\ \partial_y h &= 0, \\ \kappa &= 0. \end{aligned} \quad (3.7)$$

We impose at the contact line, at $z = z_{\text{cl}}$, that

$$\begin{aligned} h &= 0, \\ |\nabla h| &= \tan \theta_{\text{cl}}, \\ h \mathbf{U} &= \mathbf{0}. \end{aligned} \quad (3.8)$$

The first condition determines the position of the contact line, while the third condition ensures that no liquid passes the contact line. This condition is not trivial, since the equations admit solutions where the liquid velocity diverges as $\sim 1/h$. The second condition imposes the microscopic contact angle, θ_{cl} , emerging from the force balance at the contact line. This condition is actually hotly debated: for simplicity it is often assumed that this microscopic angle remains fixed at its equilibrium value (Hocking 2001, Eggers 2004), but measurements have suggested that this angle varies with Ca (Ramé et al. 2004). We will limit ourselves to presenting an argument in favour of a fixed microscopic angle. The boundary condition arises at a molecular scale, l_{vdW} , at which the fluid starts to feel the van der Waals forces exerted by the substrate. This effect can be incorporated by a disjoining pressure A/h^3 , where the Hamaker constant $A \propto \gamma l_{vdW}^2$ (Israelachvili 1992). At $h = l_{vdW}$, this yields a contribution of the order Ah'/l_{vdW}^2 in Eq. (3.3). Taking $l_{vdW} \sim l_s$, the viscous stresses will have a relative influence on the disjoining term, and thus on the boundary condition, of the order of $Ca \sim 10^{-2}$, so that the contact angle should roughly remain within 1% of its equilibrium value. This analysis of the microscopic contact angle will be extended and compared to novel experimental results in a forthcoming paper (Delon et al. 2006).

3.3. The basic profile and the bifurcation diagram

We first solve for the basic profile $h_0(z)$, corresponding to a stationary meniscus that is invariant along y . From continuity we find that hU_z is constant, which using the boundary condition Eq. (3.8) yields $U_z = 0$. The momentum balance Eq. (3.6) for $h_0(z)$ thus reduces to

$$\kappa'_0 = 1 - \frac{3Ca}{h_0(h_0 + 3l_s)}, \quad (3.9)$$

with

$$\kappa_0 = \frac{h''_0}{(1 + h_0'^2)^{3/2}}. \quad (3.10)$$

Close to the bath, i.e. $z \approx 0$, the height of the interface becomes much larger than the capillary length, so that one can ignore the viscous term. The asymptotic solution of Eq. (3.9) near $z = 0$ thus simply corresponds to that of a static bath,

$$\begin{aligned} h_0 &= -\ln z/c, \\ h'_0 &= -\frac{1}{z}, \\ \kappa_0 &= z, \end{aligned} \quad (3.11)$$

which indeed respects the boundary conditions of Eq. (3.7). This solution has one free parameter, c , that can be adjusted to fulfill the remaining boundary condition at the contact line, $h'_0 = -\tan \theta_{cl}$. It is not entirely trivial that this uniquely fixes the solution since Eq. (3.9) degenerates for $h_0 = 0$. One can show that the asymptotic solution for small $Z = z_{cl} - z$ reads (Buckingham et al. 2003)

$$h_0 = \tan \theta_{cl} Z - \frac{(1 + \tan^2 \theta_{cl})^{3/2} Ca}{2l_s \tan \theta_{cl}} Z^2 \ln Z + \tilde{c} Z^2, \quad (3.12)$$

where \tilde{c} is the sole degree of freedom. The expansion can be continued to arbitrary order once θ_{cl} and \tilde{c} are fixed.

So, the basic profile $h_0(z)$ is indeed determined by the microscopic parameters θ_{cl} and l_s , and the (experimental) control parameter Ca . This is illustrated in Fig. 4a, showing $z_{cl}(Ca)$ for fixed parameters $\theta_{cl} = 51.5^\circ$ and $l_s = 5 \cdot 10^{-7}$. Similar to Hocking 2001 and

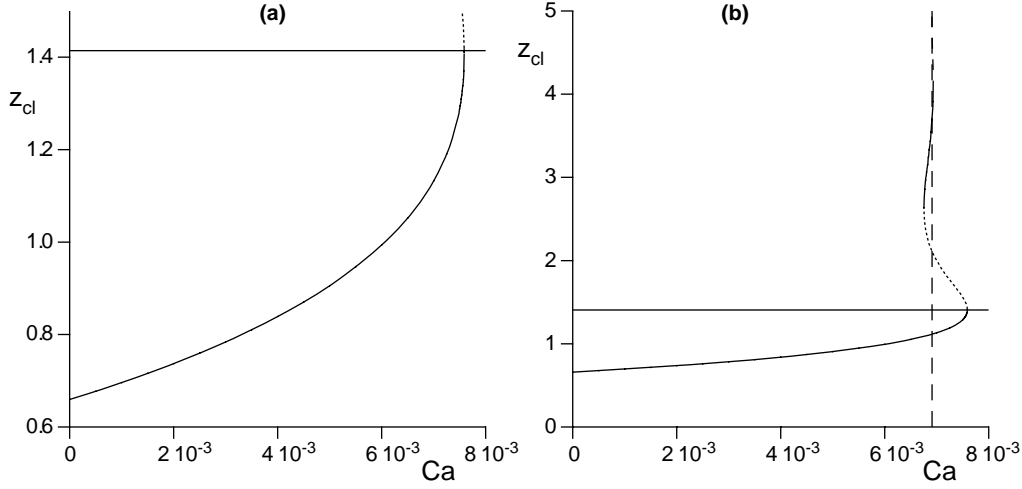
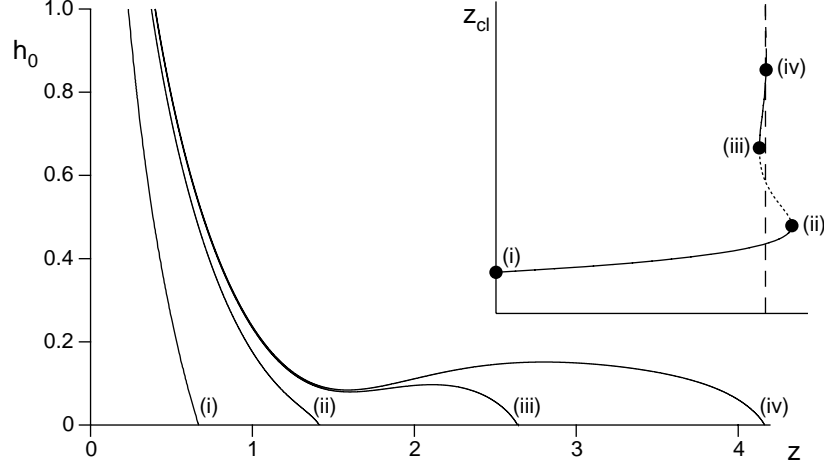


FIGURE 4. (a) Contact line position z_{cl} at equilibrium as a function of the capillary number Ca for fixed parameters $\theta_{cl} = 51.5^\circ$ and $l_s = 5 \cdot 10^{-7}$. Stationary solutions cease to exist above a critical value $Ca_c = 0.00759 \dots$. The horizontal bar denotes $z_{cl} = \sqrt{2}$. (b) Same as (a), but now showing the full range of z_{cl} . The solutions undergo a sequence of saddle-node bifurcations with ultimately $z_{cl} \rightarrow \infty$, with a corresponding $Ca^* = 0.00693 \dots$ (dashed line).

Eggers 2004, we find that stationary meniscus solutions only exist up to a critical value Ca_c . Beyond this capillary number the interface has to evolve dynamically and a liquid film will be deposited onto the plate. One can use Fig. 4a to extract the apparent contact angle θ_a , via Eq. (2.3). The critical capillary number is attained when $z_{cl} = 1.4076 \dots$, which is very close to $\sqrt{2} = 1.4142 \dots$. This confirms the predictions by Eggers 2004 that stationary solutions cease to exist at a zero apparent contact angle. This slight difference from $\sqrt{2}$ is due to the fact that Eggers's asymptotic theory becomes exact only in the limit where $l_s \rightarrow 0$, so that minor deviations can indeed be expected. Other values of θ_{cl} and l_s lead to very similar curves, always with a transition at $z_{cl} \simeq \sqrt{2}$, but with shifted values of Ca_c . This critical value roughly scales as $Ca_c \propto \theta_{cl}^3 / \ln l_s^{-1}$ (Eggers 2004, Eggers 2005).

In fact, the existence of a maximum capillary number is due to a saddle-node bifurcation, which originates from the coincidence of a stable and an unstable branch (this will be shown in more detail in Sec. 5). As can be seen from Fig. 4b, there is a branch that continues above $z_{cl} = \sqrt{2}$. Surprisingly, these solutions subsequently undergo a series of saddle-node bifurcations, with capillary numbers oscillating around a new Ca^* . This asymptotically approaches a solution of an infinitely long flat film behind the contact line. Figure 5 shows the corresponding profiles h_0 , and illustrates the formation of the film. This film is very different from the so-called Landau-Levich film, which was computed in a classic paper Landau & Levich 1942). The Landau-Levich solution is much simpler in the sense that it does not involve a contact line and does not display the non-monotonic shape shown in Fig. 5. The difference markedly shows up in the thickness of the film: while the Landau-Levich film thickness scales as $Ca^{2/3}$, the film with a contact line has a thickness $h_\infty = \sqrt{3}Ca^*$. Note that very similar film solutions were already identified by Hocking 2001 and more recently by Münch & Evans 2005 in the context of Marangoni-driven flows.

These new film solutions have indeed been recently experimentally, as transient states in the deposition of the Landau-Levich film (Snoeijer et al. 2006). In fact, the transition

FIGURE 5. Various basic solutions $h_0(z)$ along the bifurcation diagram of Fig. 4, see inset.

towards entrainment was observed to coincide at Ca^* , hence well *before* the critical point Ca_c and with $\theta_a \neq 0$. For fibres, on the other hand, the condition of vanishing contact angle has been observed experimentally by Sedev & Petrov 1991. We come back to this issue at the end of the paper.

3.4. Physical meaning of the apparent contact angle

From the definition of Eq. (2.3), it is clear that the apparent contact angle represents an extrapolation of the large scale profile using the static bath solution. In reality, however, the interface profile is strongly curved near the contact line and the contact angle increases to a much larger θ_{cl} . This has been shown in Fig. 6, revealing the logarithmic evolution of the interface slope close to the contact line. This is different from the static bath solutions, for which the slope decreases monotonically when approaching the contact line (Fig. 6b, dashed curve). Another way to define a typical contact angle in the dynamic situation could thus be to use the inflection point, which yields the minimum slope of the interface. However, when using $\theta_a(Ca)$ as an asymptotic matching condition for an outer scale solution, like in a quasi-static theory, it is clear that it only makes sense to use the extrapolated version.

4. Linear stability within the hydrodynamical model

We now turn to the actual linear stability analysis within the hydrodynamic model. This section poses the mathematical problem and addresses some technical issues related to asymptotic boundary conditions. The numerical results will be presented in Sec. 5.

4.1. Linearized equation and boundary conditions

We linearize Eqs. (3.5,3.6) about the basic profile $h_0(z)$, writing

$$h(z, y, t) = h_0(z) + \varepsilon h_1(z) e^{-\sigma t + i q y}, \quad (4.1)$$

$$\kappa(z, y, t) = \kappa_0(z) + \varepsilon \kappa_1(z) e^{-\sigma t + i q y}, \quad (4.2)$$

$$U_z(z, y, t) = \varepsilon U_{z1}(z) e^{-\sigma t + i q y}, \quad (4.3)$$

$$U_y(z, y, t) = \varepsilon U_{y1}(z) e^{-\sigma t + i q y}. \quad (4.4)$$

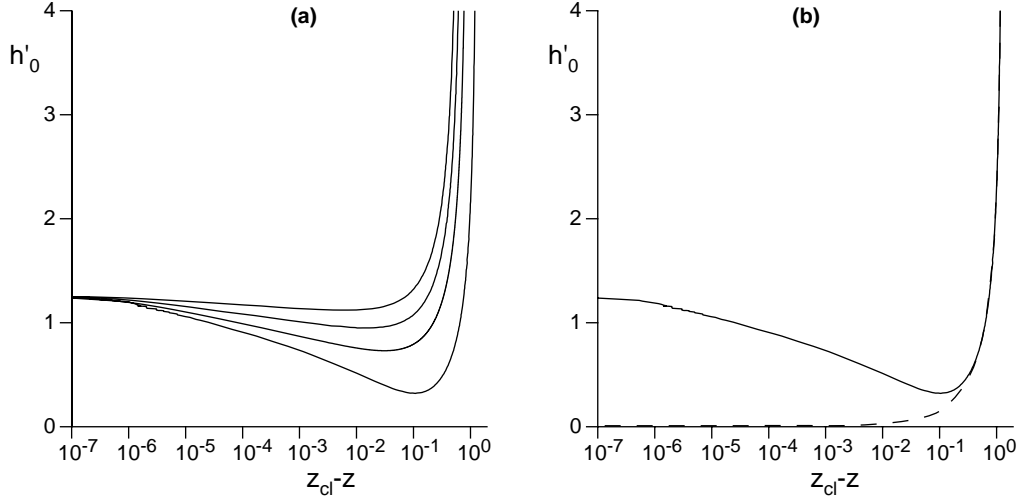


FIGURE 6. (a) Variation of the slope h'_0 as a function of the distance to the contact line, for different values of Ca . (b) The profile h'_0 for the critical solution (solid line), compared to the static bath with $\theta_a = 0$ (dashed line).

Here we used that the basic velocity $\mathbf{U}_0 = \mathbf{0}$, so that the velocity is of order ε only. The linearized equation is not homogeneous in z , due to $h_0(z)$, so the eigenmodes are nontrivial in the z direction. From the y -component of Eq. (3.6), one can eliminate U_{y1} in terms of κ_1 , as

$$U_{y1}(z) = \frac{1}{3} i q h_0 (h_0 + 3l_s) \kappa_1(z). \quad (4.5)$$

It is convenient to introduce the variable

$$F_1(z) = h_0(z) U_{z1}(z), \quad (4.6)$$

which represents the flux in the z direction at order ε (the zeroth order flux being zero). Writing the vector

$$\vec{X} = \begin{pmatrix} h_1 \\ h'_1 \\ \kappa_1 \\ F_1 \end{pmatrix}, \quad (4.7)$$

one can cast the linearized equation for the eigenmode as

$$d_z \vec{X} = \mathcal{A} \vec{X}, \quad (4.8)$$

where d_z denotes the derivative with respect to z and the right hand side is a simple matrix product. From linearization of Eqs. (3.4), (3.5), and (3.6) one finds

$$\mathcal{A} = \begin{pmatrix} 0 & 1 & 0 & 0 \\ q^2(1 + h_0'^2) & 3h_0'\kappa_0(1 + h_0'^2)^{1/2} & (1 + h_0'^2)^{3/2} & 0 \\ \frac{3Ca}{h_0^2(h_0 + 3l_s)}(2 - \frac{3l_s}{h_0 + 3l_s}) & 0 & 0 & \frac{3}{h_0^2(h_0 + 3l_s)} \\ \sigma & 0 & q^2 h_0^2(h_0 + 3l_s)/3 & 0 \end{pmatrix}.$$

The eigenmodes and corresponding eigenvalues σ_q of this linear system are determined through the boundary conditions. At the contact line, we have to obey the boundary conditions of a microscopic contact angle $\tan \theta_{cl}$ and a zero flux (see Eq. (3.8)). To translate this in terms of the linearized variables, we have to evaluate $|\nabla h|$ at the position of the contact line $z_{cl} + \Delta z$. Along the lines of App. B one finds $\Delta z = \varepsilon e^{-\sigma t + i q y} h_1 / \tan \theta_{cl}$. Linearizing $|\nabla h|$ then yields the boundary conditions for the eigenmode

$$h'_1 = -\frac{\kappa_0 (1 + h_0'^2)^{3/2}}{\tan \theta_{cl}} h_1, \quad (4.9)$$

$$F_1 = 0. \quad (4.10)$$

At the side of the bath, $z \rightarrow 0$, the conditions become

$$i q h_1 = 0 \quad \Rightarrow \quad q = 0 \quad \vee \quad h_1 = 0, \quad (4.11)$$

$$\kappa_1 = 0. \quad (4.12)$$

Below we identify the two relevant asymptotic behaviors at the bath respecting these boundary conditions.

4.2. Shooting: asymptotic behaviors at bath

The strategy of the numerical algorithm is to perform a shooting procedure from the bath to the contact line, where we have to obey the two conditions Eq. (4.9) and (4.10). We thus require two degrees of freedom, one of which is the sought for eigenvalue σ . Since the problem has been linearized, the amplitude of a single asymptotic solution does not represent a degree of freedom: one can use the relative amplitudes of two asymptotic solutions as the additional parameter to shoot towards the contact line. We thus need to identify two linearly independent solutions that satisfy the boundary boundary conditions (4.11, 4.12).

There are two asymptotic solutions of the type:

$$\begin{aligned} h_1 &= z^\alpha \left(1 + \frac{3Ca}{2(\alpha+1)^2} \frac{1}{\ln^2(z/c)} \right) \\ h'_1 &= \alpha z^{\alpha-1} \left(1 + \frac{3Ca}{2(\alpha+1)^2} \frac{1}{\ln^2(z/c)} \right) \\ \kappa_1 &= \frac{-6Ca}{\alpha+1} \frac{z^{\alpha+1}}{\ln^3(z/c)} \\ F_1 &= \frac{\sigma}{\alpha+1} z^{\alpha+1}. \end{aligned} \quad (4.13)$$

These exist for the two roots of

$$\alpha^2 + 2\alpha - q^2 = 0 \quad \Rightarrow \quad \alpha_\pm = \pm \sqrt{1 + q^2} - 1. \quad (4.14)$$

Since we want h_1 to be bounded, only the solution α_+ is physically acceptable. Interestingly, the mode $h_1 \propto z^{\alpha_+}$ precisely has the well-known Laplacian structure of $\exp(-qx + i q y)$ when transformed in the frame where the bath is horizontal – see Appendix A. This mode thus corresponds to a zero curvature perturbation of a static bath, with no liquid flow. Indeed, no flux crosses the bath since $F_1 \rightarrow 0$.

However, the motion of the contact line implies that liquid is being exchanged with the liquid reservoir, so we require an asymptotic solution that has a nonzero value of F_1 .

We found that the corresponding mode has the following structure:

$$\begin{aligned}
 h_1 &= -\frac{q^2 \mathcal{L}(z)}{z} + \frac{1}{\ln^3(z/c)} \\
 h'_1 &= \frac{q^2 \mathcal{L}(z)}{z^2} + \frac{q^2}{z \ln^3(z/c)} - \frac{3}{z \ln^4(z/c)} \\
 \kappa_1 &= q^2(1 + q^2) \mathcal{L}(z) \\
 F_1 &= \frac{1}{3} q^2(1 + q^2) .
 \end{aligned} \tag{4.15}$$

where \mathcal{L} stands for

$$\mathcal{L}(z) = \int_0^z dt \frac{-1}{\ln^3(t/c)} . \tag{4.16}$$

This integral can be rewritten in terms of a logarithmic integral using partial integration, but this does not yield a simpler expression.

For completeness, let us also provide the fourth asymptotic solution of this fourth order system:

$$\begin{aligned}
 h_1 &= \frac{1}{z} \left(1 - \frac{3\text{Ca}}{1 + q^2} \frac{1}{\ln^2(z/c)} \right) \\
 h'_1 &= -\frac{1}{z^2} \left(1 - \frac{3\text{Ca}}{1 + q^2} \frac{1}{\ln^2(z/c)} \right) \\
 \kappa_1 &= -(1 + q^2) \left(1 - \frac{3\text{Ca}}{1 + q^2} \frac{1}{\ln^2(z/c)} \right) \\
 F_1 &= \sigma \ln(z/c) ,
 \end{aligned} \tag{4.17}$$

which clearly violates the boundary conditions Eq. (4.11,4.12).

To summarize, there are two asymptotic solutions that are compatible with the boundary conditions at the bath. Their relative amplitudes can be adjusted to satisfy one of the two boundary conditions at the contact line. The numerical shooting procedure allows finding the eigenvalue σ_q for which also the second boundary condition is obeyed.

5. The dispersion relation

5.1. Numerical results

Let us now discuss the dispersion relation of contact line perturbations obtained within the hydrodynamic framework. For fixed microscopic parameters, the relaxation rate depends on the capillary number Ca and the dimensionless wave number q that has been normalized by the capillary length. This relation will be represented by the function $\sigma_q(\text{Ca})$, which has the dimension of the inverse time-scale $\gamma/(\eta l_\gamma)$. From the definition Eq. (4.1), it follows that σ is positive for stable solutions.

The dispersion relations are summarized by Fig. 7, displaying σ_q for various values of Ca . For values well below the critical speed Ca_c , one finds that the relaxation increases with q , in a manner consistent with the quasi-static prediction that $\sigma \propto |q|$ for large q . The crossover towards this linear scaling happens around $q \approx 1$, and is thus governed by the capillary length.

Close to the critical point, however, we find two unexpected features. First, it is clear from Fig. 7b that the linear regime disappears, or lies outside the range of our curves. We have not been able to extend the numerical calculation to larger values of q due

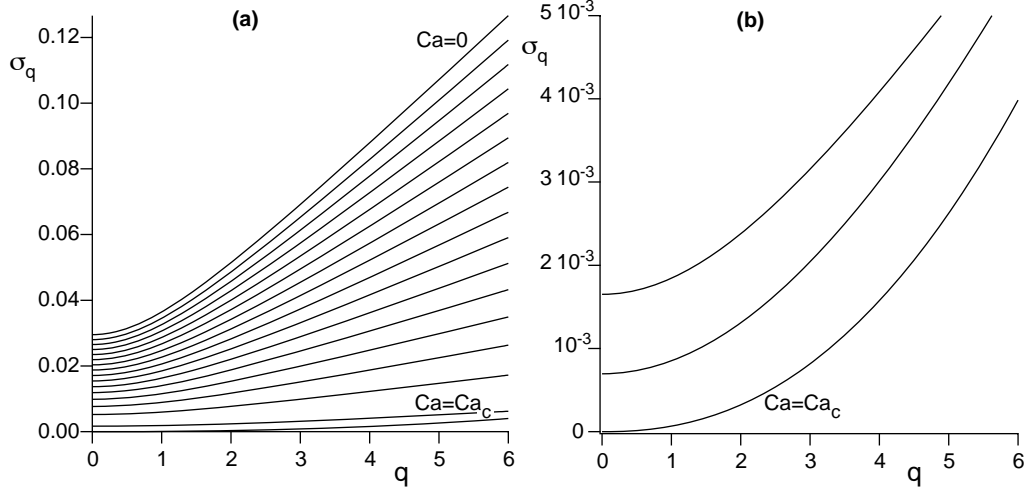


FIGURE 7. Dispersion relation obtained numerically. (a) Relaxation rates σ as a function of q , in units of $\gamma/(\eta l_\gamma)$ and $1/l_\gamma$ respectively. The various curves correspond to values of Ca ranging from 0 to 7.5×10^{-3} increasing by steps of 0.5×10^{-3} , plus Ca_c . (b) Same but close to the critical capillary number: from top to bottom, $Ca = 0.0075$, $Ca = 0.0075687$ and $Ca \simeq Ca_c = 0.00758751$.

to intrinsic instability of the numerical algorithm (the presented curves have arbitrary precision). Hence, the crossover value for q , denoted by the inverse wavelength $1/\lambda_{\text{cut}}$, increases dramatically close to the transition. Second, we observe a vanishing relaxation rate for the mode $q = 0$ at Ca_c , or equivalently a diverging relaxation time. However, the rates at *finite* wavelengths remain nonzero at the transition. This is in contradiction with the quasi-static theory, Eq. (2.7), suggesting that σ_q vanishes at all length scales at the transition.

To characterize these behaviors in more detail, it is convenient to use an empirical relation for the numerical curves (Ondarçuhu 1992),

$$\sigma_q \simeq \sigma_0 + \sigma_\infty \left(\frac{\sqrt{1 + (q\lambda_{\text{cut}})^2} - 1}{\lambda_{\text{cut}}} \right). \quad (5.1)$$

This form contains the two main features of the dispersion: the relaxation rate for the zero mode $\sigma_0(Ca)$, and the prefactor in the linear regime $\sigma_\infty(Ca) \equiv \lim_{q \rightarrow \infty} \sigma_q/q$ already defined in Eq. (2.2). The cut-off length λ_{cut} then characterizes the cross-over between the two regimes. The quasi-static prediction would be that $\lambda_{\text{cut}} \approx 1$ and $\sigma_\infty \propto \sigma_0$, see Eq. (2.9). We have found that Eq. (5.1) provides an excellent fit for all data. Only close to the critical point, where the linear regime is no longer observed within our numerical range, the values of λ_{cut} and σ_∞ are slightly dependent on the choice for the fit. The result for σ_0 is completely independent of this choice.

Let us first follow the relaxation of the mode $q = 0$ as a function of Ca . Figure 8a shows that σ_0 decreases with Ca , so that the relaxation is effectively slowed down. When approaching the critical point, this stable branch actually merges with the first unstable branch shown in Fig. 4b, the latter giving negative values for σ_0 . As a consequence, the relaxation rate has to change sign at Ca_c , so that $\sigma_0 = 0$ at this point. The graph in Fig. 8b shows that this the relaxation time diverges as $\sigma_0^{-1} \propto 1/\sqrt{Ca_c - Ca}$. As we argue below, this behavior is a fingerprint of a saddle-node bifurcation. This scenario is repeated when following the higher branches of Fig. 4b. Indeed, one finds a succession of

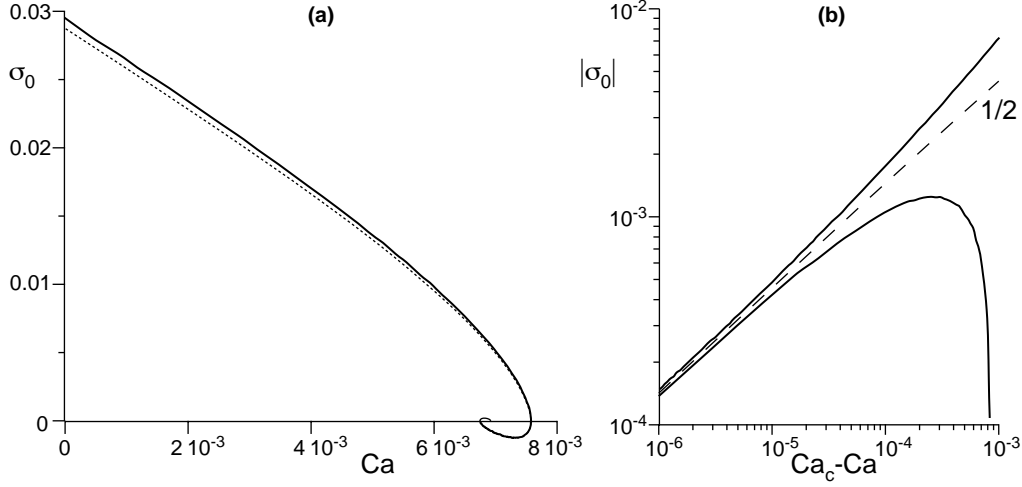


FIGURE 8. (a) Zero mode relaxation rate σ_0 as a function of Ca (solid line). The dashed line shows the quasi-static approximation. (b) Same but plotted in Log-Log coordinates as a function of $Ca_c - Ca$.

saddle-node bifurcations at which σ_0 changes sign. In Fig. 8a this manifests itself as an inward spiral, so that the solution with $z_{cl} \rightarrow \infty$ has $\sigma = 0$. The dotted curve in Fig. 8a has been obtained from the quasi-static prediction, Eq. (2.5), relating σ_0 to the curve $z_{cl}(Ca)$ displayed in Fig. 4b: the agreement is excellent.

This agreement is in striking contrast to the discrepancy at small wavelengths. These are represented in Fig. 9a through $\sigma_\infty(Ca)$. The comparison with quasi-static theory (dotted line), reveals a significant quantitative disagreement for all Ca . However, the most striking feature is that σ_∞ diverges near the transition. This suggests that for large q the relaxation rates increase faster than linearly, so that the quasi-static theory breaks down even qualitatively. A direct consequence is then that $\lambda_{cut} \rightarrow 0$, as can be seen from Fig. 9b. At the critical point Eq. (5.1) reduces to $\sigma_q \simeq \sigma_\infty \lambda_{cut} q^2/2$ for small q , so that $\lambda_{cut} \propto 1/\sigma_\infty$. These results underline the qualitative change when approaching Ca_c .

5.2. Interpretation

We propose the following interpretation for the behavior near the critical point. We have seen that the $q = 0$ mode is well described through a standard saddle-node bifurcation, which has the normal form

$$\frac{dA}{dt} = \mu - A^2. \quad (5.2)$$

For positive μ , this equation has two stationary solutions, namely $A_\pm = \pm\sqrt{\mu}$. Linear stability analysis around these solutions shows that the A_+ solutions are stable while the A_- are unstable, and the corresponding relaxation rates scale as $\sigma = \pm 2\sqrt{\mu}$. So indeed, our numerical results for $q = 0$ are described by the saddle-node normal form, when taking $\mu \propto Ca - Ca_c$ and $A = \sqrt{2} - z_{cl}$.

Making an expansion around the critical point that incorporates slow spatial variations in y , one would expect the following structure

$$\frac{\partial A}{\partial t} = \mu - A^2 + D \frac{\partial^2 A}{\partial y^2}. \quad (5.3)$$

Due to the symmetry $y \rightarrow -y$, the single derivative of y can never emerge. This then

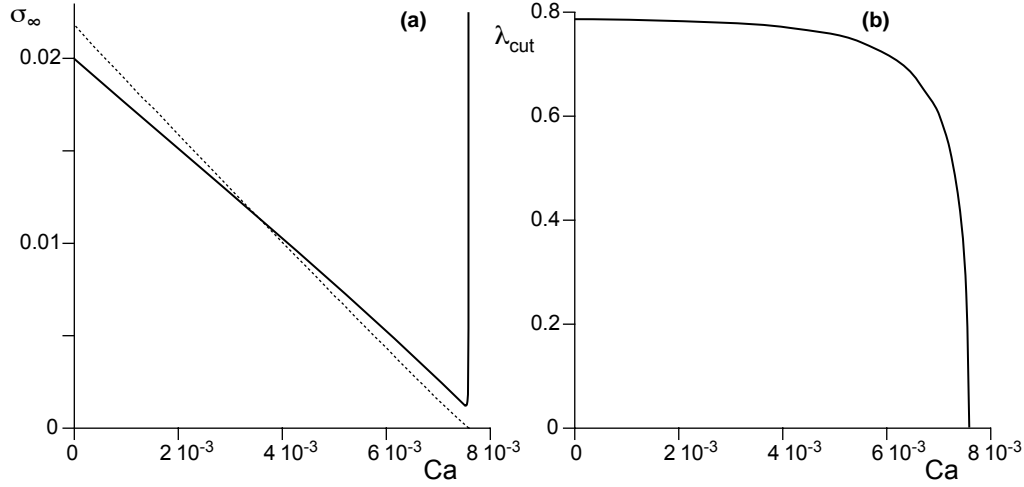


FIGURE 9. (a) Asymptotic relaxation rate $\sigma_\infty \equiv \lim_{q \rightarrow \infty} \sigma_q/q$ as a function of the capillary number Ca (solid line). The dotted line shows the quasi-steady prediction, Eq. (2.1). (b) Crossover wavelength λ_{cut} as a function of capillary number Ca .

yields a dispersion relation

$$\sigma = \sigma_0 + Dq^2 + \mathcal{O}(q^4) . \quad (5.4)$$

This explains the observation that for finite q the relaxation rates remain finite at the critical point, even though $\sigma_0 = 0$. When comparing to Eq. (5.1), one finds that $D = \sigma_\infty \lambda_{\text{cut}}/2$. This value decreases with Ca but remains finite at the transition. Interestingly, however, the dependence $D(Ca)$ appears to extrapolate to zero only about 1% beyond Ca_c .

6. Discussion

We have performed a hydrodynamic calculation of perturbed receding contact lines, in which viscous dissipation has been taken into account on all length scales (from molecular to macroscopic). This goes beyond earlier work by Golestanian & Raphael and Nikolayev & Beysens 2003, in which all dissipation was assumed to be localized at the contact line and described by an apparent (macroscopic) contact angle θ_a .

In the first part of the paper we have revealed the bifurcation diagram for straight contact lines, which turns out to be much richer than expected from the simplified quasi-static approach. Instead of a single saddle-node bifurcation at the critical capillary number Ca_c , we find a discrete series of such bifurcation points converging to a second threshold capillary number Ca^* (Fig. 4). Interestingly, the latter solutions have been observed experimentally as transient states towards liquid deposition (Snoeijer et al. 2006). These experiments showed that the wetting transition occurs already at Ca^* , and hence before the critical value Ca_c at which stationary menisci cease to exist. Since we have found the lower branch of Fig. 4 to be linearly stable at all length scales, this subcritical transition has to be mediated by some (unknown) nonlinear mechanism. Let us note that similar experiments using thin fibres instead of a plate suggest that it actually is possible to approach the critical point (Sedev & Petrov 1991). It would be interesting to investigate the bifurcation diagram as a function of the fibre radius r , where the present work represents the limit $r/l_\gamma \rightarrow \infty$.

The second part concerned the relaxation of perturbed contact lines. At long wave-

lengths, $ql_\gamma \ll 1$, we have found that the relaxation obtained in the hydrodynamic calculation is very close to the quasi-static prediction. The quasi-static model is based upon the equilibrium contact line position at steady-state, as a function of the capillary number: it treats the perturbations as a small displacement of the contact line, Δz_{cl} , that induces a change in the contact line velocity $\sim dCa/dz_{cl}$. A positive (negative) derivative indicates that the contact line is stable (unstable). This argument does not involve the apparent contact angle: it holds as long as the interface profile relaxes adiabatically along *stationary* or *steady* meniscus solutions. The long wavelength theory therefore relies on a "quasi-steady" assumption, and not so much on the interface being nearly at equilibrium (quasi-static). We wish to note that the physics is slightly different for a contact line on a horizontal plane, for which there is no equilibrium position due to gravity. For an infinite volume translational invariance implies that $\sigma_0 = 0$ (Sekimoto et al. 1987), while drops of finite volume has a finite resistance to long wave-length perturbations. This nicely illustrates the importance of the outer geometry.

For small wavelengths, $ql_\gamma \gg 1$, we found that the quasi-static theory breaks down. Away from the critical point we still observe the scaling $\sigma \propto |q|$, as proposed by Joanny & de Gennes 1984. This scaling reflects the "elasticity" of contact lines, representing an increase of surface area, and thus of the surface free energy, proportional to $|q|$. Quantitatively, however, the quasi-static approximation is not able to capture the hydrodynamic calculation. The disagreement becomes even *qualitative* close to the critical point: finite wavelength perturbations do not develop the diverging relaxation times predicted by Golestanian & Raphael 2001a. Also, the scaling $\sigma \propto |q|$ is found to cross over to a quadratic scaling $\sigma \propto q^2$.

These results have a clear message: viscous effects have to be treated explicitly when describing spatial structures below the capillary length. Namely, the viscous term in Eq. (3.3) becomes at least comparable to gravity at this scale. Therefore one can no longer assume that viscous effects are localized in a narrow zone near the contact line: the perturbations become comparable to the size of this viscous regime. However, even if contact line variations are slow, a complete description still requires a prediction for $z_{cl}(Ca)$, or equivalently $\theta_a(Ca)$. As was shown by Eggers 2004, this relation is not geometry-independent so one can never escape the hydrodynamic calculation.

Our findings provide a detailed experimental test that, on a quantitative level, are relatively sensitive to the microscopic physics near at the contact line. In our model we have used a simple slip law to release the singularity, but a variety of other mechanisms have been proposed previously. The other model parameter is the microscopic contact angle θ_{cl} , which we have simply taken constant in our calculations. In a forthcoming paper we present experimental results and show to what extent the model is quantitatively accurate for the dynamics of contact lines.

Acknowledgements – We wish to thank J. Eggers for fruitful discussions and P. Brunet for useful suggestions on the manuscript. JHS acknowledges financial support by a Marie Curie European Fellowship FP6 (MEIF-CT2003-502006).

Appendix A. Perturbation of the static bath away from the plate

At large distances from the plate, the behavior of the static bath is more conveniently described through the function $z_{\text{surface}}(x, y) = \hat{z}(x, y)$. Denoting x positive away from the plate, we find asymptotically that $\hat{z} = \hat{z}' = \hat{z}'' = 0$ as $x \rightarrow \infty$. The equation for the static interface then simplifies to

$$\nabla^2 \hat{z} = \hat{z}, \quad (\text{A } 1)$$

where we have put $l_\gamma = 1$. The basic profile is simply exponential

$$\hat{z}_0 = Ae^{-x}, \quad (\text{A } 2)$$

while transverse perturbations e^{iqy} decay along x as

$$\hat{z}_1 = e^{-\sqrt{1+q^2}x}. \quad (\text{A } 3)$$

We can thus write

$$\hat{z} = Ae^{-x} + \varepsilon e^{iqy}(e^{-x})^{\sqrt{1+q^2}}, \quad (\text{A } 4)$$

and compare this to the representation $x_{\text{surface}} = h(z, y)$

$$h = -\ln(z/c) + \varepsilon e^{iqy} h_1(z). \quad (\text{A } 5)$$

Inserting this $x = h(z, y)$ in Eq. (A 4), and identifying $\hat{z} = z$, we obtain to lowest order in ε

$$z = \frac{Az}{c}(1 - \varepsilon e^{iqy} h_1(z)) + \varepsilon e^{iqy} \left(\frac{Az}{c}\right)^{\sqrt{1+q^2}}, \quad (\text{A } 6)$$

so that $A/c = 1$ and $h_1(z) = z^\alpha$, with $\alpha = \sqrt{1+q^2} - 1$. So, the exponential relaxation in the frame (x, y) translates into a power law for $h_1(z)$.

Appendix B. Quasi-static approximation

In this appendix we derive the quasi-static results summarized in Sec. 2. To perform a linear stability analysis, we write the interface profile as

$$h(z, y, t) = h_0(z) + \varepsilon h_1(z) e^{-\sigma t + iqy}, \quad (\text{B } 1)$$

$$\kappa(z, y, t) = \kappa_0(z) + \varepsilon \kappa_1(z) e^{-\sigma t + iqy}, \quad (\text{B } 2)$$

where κ is twice the mean curvature of the interface. In the quasi-static approach, the basic profile $h_0(z)$ can be solved from a balance between capillary forces and gravity, so that the scale for interface curvatures is the capillary length $l_\gamma = \sqrt{\gamma/\rho g}$. If we consider modulations of the contact line with short wavelengths, $1/q \ll l_\gamma$, one can thus locally treat the unperturbed profile as a straight wedge, $h_0(z) = (z_{\text{cl}} - z) \tan \theta_a$, where the position of the contact line is denoted by z_{cl} . Since gravity plays no role at these small length scales, one can easily show that the perturbation should have zero curvature, i.e. $\kappa_1(z) = 0$. In the limit of small contact angles, for which we can simply write

$$\kappa_1 \simeq \nabla^2(h_1(z) e^{-\sigma t + iqy}), \quad (\text{B } 3)$$

one directly finds that $\kappa_1 = 0$ leads to a perturbation decaying exponentially along z , as $h_1(z) = e^{-|q|(z_{\text{cl}} - z)}$. The length scale of the perturbation is then simply $1/q$. This can be generalised using the full curvature expression Eq.(3.4): inserting the linearization Eq. (B 1), and taking $\partial_z h_0 = \tan \theta_a$, $\partial_{zz} h_0 = 0$, one finds

$$\kappa_1 = (\cos \theta_a)^{3/2} \left(\partial_{zz} h_1 - \frac{q^2}{\cos^2 \theta_a} h_1 \right). \quad (\text{B } 4)$$

Hence, the condition that $\kappa_1 = 0$ yields:

$$h_1(z) = e^{-|q| \frac{z_{\text{cl}} - z}{\cos \theta_a}}. \quad (\text{B } 5)$$

From Fig. 3a it is clear that the "advanced" part of the contact line, with positive Δz ,

has a smaller apparent contact angle than the wedge. The remaining task is to relate the quantities ε , Δz and $\Delta\theta$, and to impose the correct boundary condition through $\theta_a(\text{Ca})$. We now introduce the representation

$$h(z, y, t) = h_0(z - \Delta z) + \varepsilon \hat{h}_1(z - \Delta z) e^{-\sigma t + i q y}, \quad (\text{B } 6)$$

in which the position of the contact line is explicitly shifted to $z = z_{\text{cl}} + \Delta z$, so that $\hat{h}_1(z_{\text{cl}}) = 0$. Linearizing this equation around $z = z_{\text{cl}}$, this can be written as

$$\begin{aligned} h(z, y, t) &= h_0(z) + \varepsilon \left(\hat{h}_1(z) e^{-\sigma t + i q y} - \left[\frac{dh_0}{dz} \right]_{z=z_{\text{cl}}} \frac{\Delta z}{\varepsilon} \right) + \mathcal{O}(\varepsilon^2) \\ &= h_0(z) + \varepsilon \left(\hat{h}_1(z) e^{-\sigma t + i q y} + \tan \theta_a \frac{\Delta z}{\varepsilon} \right) + \mathcal{O}(\varepsilon^2). \end{aligned} \quad (\text{B } 7)$$

Comparing to Eq. (B 1) with $h_1(z_{\text{cl}}) = 1$, one thus finds that to lowest order $\Delta z = \varepsilon e^{-\sigma t + i q y} / \tan \theta_a$. Writing $\partial h / \partial z = -(\tan \theta_a + \Delta \tan \theta)$, one furthermore finds from Eq. (B 1)

$$\Delta \tan \theta = -\frac{|q|}{\cos \theta_a} \varepsilon e^{-\sigma t + i q y} = -|q| \frac{\tan \theta_a}{\cos \theta_a} \Delta z. \quad (\text{B } 8)$$

The final step is to use the empirical relation between θ_a and Ca to relate the variation in contact angle to a variation in the contact line velocity, $U_{\text{cl}} = U - d\Delta z/dt$:

$$\begin{aligned} \frac{d\Delta z}{dt} &= -\frac{\gamma}{\eta} \Delta \text{Ca} = -\frac{\gamma}{\eta} \left(\frac{d \tan \theta_a}{d \text{Ca}} \right)^{-1} \Delta \tan \theta \\ &= \frac{|q| \gamma}{\eta} \frac{\tan \theta_a}{\cos \theta_a} \left(\frac{d \tan \theta_a}{d \text{Ca}} \right)^{-1} \Delta z. \end{aligned} \quad (\text{B } 9)$$

This indeed results into an exponential relaxation $\Delta z \propto e^{-\sigma t}$ with a relaxation rate given by Eq. (2.1).

For contact angles close to $\pi/2$, one can analytically solve the crossover from small to large wavelengths (Nikolayev & Beysens 2003). In this case the basic profile is nearly flat in the x direction. Characterizing the free surface by $z_{\text{surface}}(x, y)$, one easily finds that perturbations of the contact line decay along x over a distance $1/\sqrt{q^2 + 1/l_\gamma^2}$ – see Appendix A. Hence,

$$\frac{\sigma_q}{\sigma_0} \simeq \sqrt{1 + (ql_\gamma)^2} \quad \text{for } \theta_a \approx \pi/2. \quad (\text{B } 10)$$

This is consistent with Eq. (2.7), since $g(\pi/2) = 1$.

REFERENCES

- BARRAT, J.-L. & BOCQUET, L. 1999 Large Slip Effect at a Nonwetting Fluid-Solid Interface. *Phys. Rev. Lett.* **82**, 4671-4674.
- BLAKE, T.D., CONINCK J. DE & D'ORTUNA U. 1995 Models of wetting: Immiscible lattice Boltzmann automata versus molecular kinetic theory. *Langmuir* **11**, 4588.
- BLAKE, T.D. & RUSCHAK K.J. 1979 A maximum speed of wetting. *Nature* **282**, 489-491.
- BUCKINGHAM, R., SHEARER, M. & BERTOZZI, A. 2003 Thin film traveling waves and the Navier-slip condition. *SIAM J. Appl. Math.* **63**, 722-744.
- COTTIN-BIZONNE, C., CROSS, B., STEINBERGER, A. & CHARLAIX, E. 2005 Boundary Slip on Smooth Hydrophobic Surfaces: Intrinsic Effects and Possible Artifacts. *Phys. Rev. Lett.* **94**, 056102.
- COX, R.G. 1986 The Dynamics of the spreading of liquids on a solid surface. *J. Fluid Mech.* **168**, 169-194.

- DELON, G., FERMIGIER, M., SNOEIJER J.H., & ANDREOTTI, B. in preparation.
- DUSSAN, E.B., DAVIS, V. & DAVIS, S.H. 1974 On the motion of a fluid-fluid interface along a solid surface. *J. Fluid Mech.* **65**, 71-95.
- EGGERS, J. 2004 Hydrodynamic theory of forced dewetting. *Phys. Rev. Lett.* **93**, 094502.
- EGGERS, J. 2005 Existence of receding and advancing contact lines. *Phys. Fluids* **17**, 082106.
- JOANNY, J. -F. & GENNES, P.-G. DE 1984 Model for contact angle hysteresis. *J. Chem. Phys.* **11**, 552-562.
- GENNES, P.-G. DE 1986 Deposition of Langmuir-Blodgett layers. *Colloid Polym. Sci.* **264**, 463-465.
- GOLESTANIAN, R. & RAPHAEL, E. 2001 Dissipation in dynamics of a moving contact line. *Phys. Rev. E* **64**, 031601.
- GOLESTANIAN, R. & RAPHAEL, E. 2001 Relaxation of a moving contact line and the Landau-Levich effect. *Europhys. Lett.* **55**, 228-234.
- GOLESTANIAN, R. & RAPHAEL, E. 2003 Roughening transition in a moving contact line. *Phys. Rev. E* **67**, 031603.
- HOCKING, L.M. 2001 Meniscus draw-up and draining. *Euro. J. Appl. Math* **12**, 195-208.
- HOFFMAN, R.L. 1975 Dynamic contact angle. *J. Colloid Interface Sci.* **50**, 228-241.
- HUH, C. & SCRIVEN, L.E. 1971 Hydrodynamic model of steady movement of a solid/liquid/fluid contact line. *J. Colloid Interface Sci.* **35**, 85-101.
- HUPPERT, H. E. 1982 Flow and instability of a viscous gravity current down a slope. *Nature* **300**, 427-429.
- ISRAELACHVILI, J. 1992 Intermolecular and Surface Forces. Academic.
- LANDAU, L.D. AND LEVICH, B.V. 1942 Dragging of a liquid by a moving plate. *Acta Physicochim. URSS* **17**, 42-54.
- LANDAU, L.D. AND LIFSHITZ, E.M. 1959 Fluid Mechanics. Pergamon, London.
- LE GRAND, N., DAERR, A. & LIMAT, L. 2005 Shape and motion of drops sliding down an inclined plane. *J. Fluid Mech.* **541**, 293-315.
- MÜNCH, A. & EVANS, P.L. 2005 Marangoni-driven liquid films rising out of a meniscus onto a nearly horizontal substrate. *Physica D* **209**, 164-177.
- NIKOLAYEV, V.S. & BEYSENS, D.A. 2003 Equation of motion of the triple contact line along an inhomogeneous interface. *Europhys. Lett.* **64**, 763-768.
- ONDARÇUHU, T. & VEYSSIÉ, M. 1991 Relaxation modes of the contact line of a liquid spreading on a surface. *Nature* **352**, 418-420.
- ONDARÇUHU, T. 1992 Relaxation modes of the contact line in situation of partial wetting. *Mod. Phys. Lett. B* **6**, 901-916.
- ORON, A., DAVIS, S. H. & BANKOFF, S. G. 1997 Long-scale evolution of thin liquid films. *Rev. Mod. Phys.* **69**, 931-980.
- PIT, R., HERVET, H. & LÉGER, L. 2000 Interfacial Properties on the Submicron Scale. *Phys. Rev. Lett.* **85**, 980-983.
- PISMEN, L. M. & POMEAU, Y. 2000 Disjoining potential and spreading of thin liquid layers in the diffuse-interface model coupled to hydrodynamics. *Phys. Rev. E* **62**, 2480-2492.
- PODGORSKI, T., FLESSELLES, J. M. & LIMAT, L. 2001 Corners, cusps and pearls in running drops 2001. *Phys. Rev. Lett.* **87**, 036102.
- RAMÉ, E., GAROFF, S. & WILLSON, K.R. 2004 Characterizing the microscopic physics near moving contact lines using dynamic contact angle data. *Phys. Rev. E* **70**, 0301608.
- RIO, E., DAERR, A., ANDREOTTI, B. & LIMAT, L. 2005 Boundary conditions in the vicinity of a dynamic contact line: experimental investigation of viscous drops sliding down an inclined plane. *Phys. Rev. Lett.* **94**, 024503.
- SEDEV, R.V. & PETROV, J.G. 1991 The critical condition for transition from steady wetting to film entrainment. *Colloids and Surfaces* **53**, 147-156.
- SEKIMOTO, K., OGUMA, R. & KAWASAKI, K. 1987 Morphological stability analysis of partial wetting. *Ann. Phys.* **176**, 359-392.
- SNOEIJER, J. H., DELON, G., FERMIGIER, M. & ANDREOTTI, B. 2006 Avoided critical behavior in dynamically forced wetting, *Phys. Rev. Lett.* **96**, 174504
- THOMPSON, P.A. & ROBBINS, M.O. 1989 Simulations of contact-line motion: slip and the dynamic contact angle. *Phys. Rev. Lett.* **63**, 766-769.

Relaxation of a dewetting contact line Part 1: A full-scale hydrodynamic calculation 21

QUÉRÉ D. 1991 On the minimal velocity of forced spreading in partial wetting. *C.R. Acad. Sci. Paris II* **313**, 313-318.

VOINOV, O.V. 1976 Hydrodynamics of wetting. *Fluid Dynamics* **11**, 714-721.